JOURNAL OF SPACECRAFT AND ROCKETS
Vol. 38, No. 1, January–February 2001

Roll Effects on Carryover for Hypersonic Delta Fin Missiles

H. F. Nelson*
University of Missouri–Rolla, Rolla, Missouri 65409-0050

An Euler code is used to predict hypersonic missile flowfields and to determine the carryover factors for the effect of the body on wing lift $K_{W(B)}$ and for the effect of the wing on body lift $K_{B(W)}$. Results are presented for Mach 4, 6, 8, and 10 at an angle of attack of 2 deg. The missile has a conical nose, a cylindrical fuselage with a 1-deg flare angle, and delta fins. Both × and + fin configurations are considered. Results are given for 20- and 30-deg semivertex angles as a function of finspan to body radius (at fin leading edge), S/R_{LE}. The wing–body carryover for × fins is smaller for the top set of fins than it is for the bottom set of fins. The value of $K_{W(B)}$ for the missile with × fins is slightly larger than it is for + fins at Mach 8 and 10. At Mach 4 and 6, $K_{W(B)}$ is independent of fin configuration. $K_{B(W)}$ is larger for × fins than it is for + fins, and it increases as semivertex angle decreases from 30 to 20 deg. $K_{B(W)}$ generally decreases as both Mach number and finspan increase. Equations and tables are presented for the carryover factors.

Nomenclature

A_F	=	planform area of one fin ($A_W/2$), m^2
AR	=	aspect ratio of wing formed by joining two fins at their root chord
A_W	=	wing-planform area formed by two fins joined at their root chord, m^2
C_L	=	lift coefficient referenced to A_W
C_{L_B}	=	lift coefficient, body alone
$C_{L_{B,\alpha}}$	=	lift curve slope, body alone
C_{L_M}	=	lift coefficient, entire missile
C_{L_W}	=	lift coefficient, wing alone
$C_{L_{W,\alpha}}$	=	lift curve slope, wing alone
$F_{N,i}$	=	normal force on ith fin, N
$K_{B(W)}$	=	body–fin carryover
$K_{F(B),i}$	=	fin–body carryover on ith fin
$K_{W(B)}$	=	wing–body carryover
$K^B_{W(B)}$	=	wing–body carryover (fins 3 plus 4)
$K^T_{W(B)}$	=	wing–body carryover (fins 1 plus 2)
L_B	=	lift, body alone, N
$L_{B(W)}$	=	body lift in presence of fins, N
$L_{F(B),i}$	=	lift of ith fin in presence of body, N
L_M	=	lift, entire missile, N
L_W	=	wing-alone lift ($\Theta = 0$), N
M_∞	=	freestream Mach number
P	=	pressure/(freestream pressure)
q_∞	=	freestream dynamic pressure, N/m^2
R	=	body radius at end of nosecone, m
R_{LE}	=	body radius at root chord leading edge (1.419R), m
S	=	finspan, from body centerline, m
Z	=	missile axial distance, from nose, m
Z_{LE}	=	root-chord leading edge position, m
α_{eq}	=	equivalent angle of attack, deg
α_F	=	fin angle of attack, deg
α_∞	=	missile angle of attack, deg
ϵ	=	fin semivertex angle (20, 30 deg)
Θ	=	fin angular position (0, 45 deg)
θ_f	=	body flare angle (1 deg)
ϕ	=	body angular position, deg (0 at top)

Introduction

CONCEPTUAL and preliminary missile design has evolved from using slender body theory (SBT) and linear potential theory (LPT) to the development of the equivalent angle-of-attack method.[1] Missiles are also designed using using semi-empirical approaches, such as the aeroprediction code AP98[2,3] and Missile DATCOM,[4] which are based on extensive databases. Dillenius et al.[5] recently reviewed numerical prediction methods for missile aerodynamics.

Cruciform missiles fly in either the + fin position or the × cross-fin orientation. Figure 1 shows these fin positions. In Ref. 2 it is stated that 1) the + configuration ($\Theta = 0$ deg) is roll stabilized and generally gives a slightly larger lift force and a slightly more stable pitching moment than the × configuration ($\Theta = 45$ deg) and 2) the × fined missiles require less energy than the + finned missiles to maintain a constant roll orientation. The + orientation has negligible fin–fin interference. In the × orientation, the flowfield near fin 1 is influenced by fin 4.

The objective of this paper is to use the ZEUS code[6] to predict the hypersonic flowfield and to evaluate the hypersonic fin–body and body–fin carryover factors, $K_{W(B)}$ and $K_{B(W)}$ as functions of fin size, M_∞, and ϵ for × and + fin orientations. ZEUS allows one to investigate a wide range of configurations and flight parameters and to obtain detailed flowfield information not attainable with empirical techniques. The data generated in this research project can be used to improve the database for Missile DATCOM and semi-empirical methods.

Numerical predictions of $K_{W(B)}$ and $K_{B(W)}$ using the Euler equations have been done for hypersonic missiles in the + fin configuration.[7] The Euler equations significantly reduce computer runtime relative to the Navier–Stokes equations without degrading the quality of the results for forces and moments at low angle of attack.[8] The Euler equations allow for shock and expansion waves and account for vorticity and rotational effects; therefore, the Euler equations allow the computational modeling of the carryover factors to be a function of M_∞, ϵ, and α_∞ in addition to S/R.

Equivalent Angle of Attack

The equivalent angle of attack model is a component buildup method that considers lift on individual missile components separately and then adds the individual lifts to find the total missile lift coefficient. Carryover factors are used to account for the mutual interference between components. The lift on the four-fin missile configuration is

$$L_M = L_{B(W)} + \sum_{i=1}^{4} L_{F(B),i}$$

$$= L_B + \sum_{i=1}^{4} L_{F(B),i} + \left(L_{B(W)} - L_B\right) \qquad (1)$$

Presented as Paper 2000-0388 at the 38th Aerospace Sciences Meeting, Reno, NV, 10–13 January 2000; received 1 March 2000; revision received 10 July 2000; accepted for publication 27 July 2000.

*Professor of Aerospace Engineering, Thermal Radiative Transfer Group, Department of Mechanical and Aerospace Engineering and Engineering Mechanics. Associate Fellow AIAA.

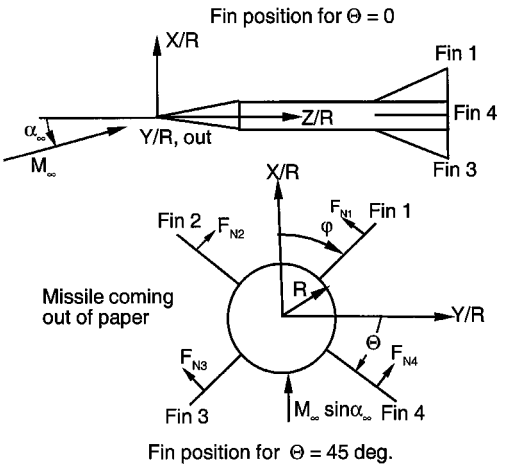

Fig. 1 Missile nomenclature.

Dividing and multiplying by L_W yields

$$L_M = L_B + \left[\sum_{i=1}^{4} \frac{L_{F(B),i}}{L_W} + \frac{L_{B(W)} - L_B}{L_W}\right] L_W \tag{2}$$

For zero yaw angles, one has $L_{F(B),1} = L_{F(B),2}$ and $L_{F(B),3} = L_{F(B),4}$. However, the lift on fins 1 and 2 is different than the lift on fins 3 and 4. To be consistent with previous work,[2] define the carryover factor for fin lift in the presence of the body for the top fins as

$$K^T_{W(B)} = \left[L_{F(B),1} + L_{F(B),2}\right]/L_W = 2L_{F(B),1}/L_W \tag{3}$$

and for the bottom fins as

$$K^B_{W(B)} = \left[L_{F(B),3} + L_{F(B),4}\right]/L_W = 2L_{F(B),4}/L_W \tag{4}$$

For × fins located symmetrically around the body, fins 1 and 3 make a wing when they are attached at their root chords and likewise for fins 2 and 4. The wing–body carryover factor $K^T_{W(B)}$ is defined as the missile lift produced by fins 1 and 2 in the presence of the body divided by the lift produced by the wing alone at $\Theta = 0$ deg. Likewise, $K^B_{W(B)}$ is defined as the missile lift produced by fins 3 and 4 in the presence of the body divided by the lift produced by the wing alone at $\Theta = 0$ deg.

The body–wing carryover $K_{B(W)}$ (due to pressure bleeding over from the wing to the body and upwash) is defined as the difference between the lift produced by the body in the presence of the fins and the lift produced by the body alone divided by the lift produced by the wing alone:

$$K_{B(W)} = \left[L_{B(W)} - L_B\right]/L_W \tag{5}$$

Note that $K_{B(W)}$ is zero except where the fins influence the lift produced by the body.

Equation (2) can be written in terms of the carryover factors as

$$L_M = L_B + \left[K^T_{W(B)} + K^B_{W(B)} + K_{B(W)}\right] L_W \tag{6}$$

Hence, the lift on the missile configuration consists of the lift on the body alone, L_B, and the lift on the wing alone, L_W, modified by the carryover factors $K^T_{W(B)}$, $K^B_{W(B)}$, and $K_{B(W)}$. The parameters $K^T_{W(B)}$ and $K^B_{W(B)}$ are normally defined in terms of the missile normal force, but at low angles of attack, the missile lift is essentially equal to the missile normal force. Accurate functional equations for $K^T_{W(B)}$, $K^B_{W(B)}$, and $K_{B(W)}$ are used in conceptual and preliminary design.

The equivalent angle-of-attack coefficient is defined by dividing Eq. (6) by $q_\infty A_W$ to get

$$C_{L_M} = C_{L_B} + \left[K^T_{W(B)} + K^B_{W(B)} + K_{B(W)}\right] C_{L_W} \tag{7}$$

The crossflow Mach number parameter $M_\infty \sin\alpha_\infty$ is less than one for all of the cases considered in this research, and so q_∞ can be used to define the lift coefficient.[9] At Mach 10 and $\alpha_\infty = 2$ deg, this parameter is 0.35.

At small angles of attack, C_L is linear with α_∞, so that $C_L = \alpha_\infty C_{L,\alpha}$ and Eq. (7) becomes

$$C_{L_M} = C_{L_{B,\alpha}} \alpha_\infty + C_{L_{W,\alpha}} \alpha_{\text{eq}} \tag{8}$$

where the equivalent angle of attack is defined as

$$\alpha_{\text{eq}} = \left[K^T_{W(B)} + K^B_{W(B)} + K_{B(W)}\right] \alpha_\infty \tag{9}$$

Reference 2 defines the entire missile $K_{W(B)}$ as

$$K_{W(B)} = K^T_{W(B)} + K^B_{W(B)} \tag{10}$$

The definition of α_{eq} becomes more complicated if sideslip, vorticity, fin deflection, multiple sets of fins, or large α_∞ are considered.[1]

Experimental Data

Missile design experimental data consist of fin-alone, body-alone, and entire-missile wind-tunnel measurements. Stallings and Lamb[10] carried out a systematic investigation of fin-alone forces for Mach numbers from 1.60 to 4.60 and angles of attack up to 60 deg. The fins had aspect ratios of 0.5, 1.0, and 2.0 and taper ratios of 0, 0.5, and 1. Burns and Bruns[11] made wind-tunnel measurements of forces on fin–body models with aspect ratios between 1 and 6 and taper ratios of 0 and 0.5 from Mach 0.6 to 3.95 for angles of attack from −2 to 30 deg. Fin–body data are available from the Tri-Service Missile database; however, it is not completely reduced and correlated.[12] Nielsen[13] analyzed some Tri-Service Missile data to extract values of $K_{W(B)}$ and $K_{B(W)}$ at Mach numbers between 2.5 and 4.5 for angles of attack from 0 to 40 deg.

Analysis

Missile Geometry

The missile geometry used in this research is shown in Figs. 1 and 2. The missile has a conical nose ending at $Z/R = 6$ and a cylindrical body with a 1-deg flare. The fin leading edge was located at $Z/R = 30$. The fins were infinitely thin flat plates with triangular planforms. Two semivertex angles were considered, $\epsilon = 20$ and 30 deg. The aspect ratio for two delta fins joined at their root chord to form a planar wing is

$$\text{AR} = \frac{4\tan^2\epsilon}{\tan\epsilon - \tan\theta_f} \tag{11}$$

Because ZEUS is an axial marching code, one run includes a series of S/R ratios. In other words, at each Z/R value greater than 30, each axial step yields a new solution for a missile with larger fins. R_{LE} is the body radius at $Z/R = 30$ ($R_{\text{LE}}/R = 1 + 24\tan\theta_f = 1.419$). S/R_{LE} is used as the independent variable for $K_{W(B)}$ and $K_{B(W)}$. Results are presented for fins varying in size from $S/R_{\text{LE}} = 1$ to 5.

Body-Alone Lift, L_B

The body-alone lift is needed to evaluate $K_{B(W)}$. SBT defines L_B as $L_B = 2\pi q_\infty \alpha_\infty R^2$ (Ref. 14). In this research, the value of L_B was

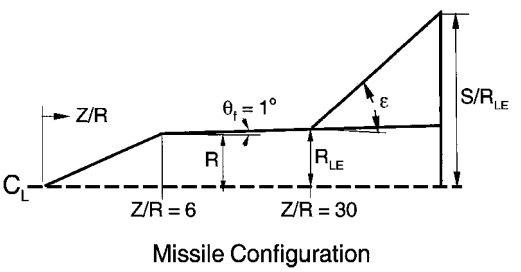

Fig. 2 Missile configuration.

determined using ZEUS. The ZEUS data for $M_\infty = 4$, 6, 8, and 10 were fit to a single linear equation (accurate to $\pm 0.3\%$) in terms of Z/R, giving

$$C_{L_B} = 0.2478 + 0.01163 Z/R \tag{12}$$

for $30 \le Z/R \ge 50$, where C_{L_B} is based on a reference area of 1 m^2. In other words, $L_B = q_\infty C_{L_B}$.

Wing-Alone Lift, L_W

The wing alone is formed by two infinitely thin fins connected at their root chord. The nondimensional wing planform area in terms of Z/R is

$$A_W = (Z - Z_{\rm LE})^2 (\tan\epsilon - \tan\theta_f) \Big/ R^2 \tag{13}$$

and in terms of $S/R_{\rm LE}$ is

$$A_W = \frac{(S/R_{\rm LE} - 1)^2}{\tan\epsilon} \left(1 - \frac{\tan\theta_f}{\tan\epsilon}\right) \left(\frac{R_{\rm LE}}{R}\right)^2 \tag{14}$$

for $Z \ge Z_{\rm LE}$. The value of L_W for the wing alone with supersonic leading edges is[14]

$$L_W = \frac{4\alpha_\infty q_\infty A_W}{\sqrt{M_\infty^2 - 1}} \tag{15}$$

Fins with subsonic edges were not considered. The wing alone is orientated at $\Theta = 0$ deg. Reference 2 also uses this wing-alone orientation.

Small Fin Limit

In the limit when the fins become vanishingly small, the values of $K_{F(B),i}$ can be predicted using LPT. In cylindrical coordinates, LPT gives the angular velocity at angle Θ on the body as

$$V(\Theta) = 2V_c \cos\Theta \tag{16}$$

where $V_c = V_\infty \sin\alpha_\infty \approx V_\infty \alpha_\infty$ is the crossflow velocity. The missile lift force produced by the fin is $4\alpha_F q_\infty A_F \cos\Theta / \sqrt{(M_\infty^2 - 1)}$, where $\alpha_F = V(\Theta)/V_\infty = 2\alpha_\infty \cos\Theta$. Likewise, the lift of the wing alone is $4\alpha_\infty q_\infty A_W / \sqrt{(M_\infty^2 - 1)}$, where $\alpha_\infty = V_c / V_\infty$. The value of $K_{F(B),i}$ is equal to the missile lift produced by fin i divided by the lift produced by the wing alone. Thus, $K_{F(B),i} = \cos^2\Theta_i$. Hence, from Eqs. (3) and (4)

$$K^T_{W(B)} = 2\cos^2\Theta, \qquad K^B_{W(B)} = 2\cos^2\Theta \tag{17}$$

for vanishingly small fins. Note for $\Theta = 0$ deg (+ fin configuration) only one of the $K_{W(B)}$ equations is valid and that it goes to 2 (in agreement with SBT). At $\Theta = 45$ deg, both $K^T_{W(B)}$ and $K^B_{W(B)}$ go to 1.

Methodology

ZEUS is a finite volume Euler code (developed by the U.S. Naval Surface Weapons Center[6]) that solves the three-dimensional Euler equations by marching axially along the missile using a multiple zone grid in the cross-sectional plane. Flowfield solutions were obtained between the body and the bow shock. A large number of r points were used to maintain good accuracy. A uniform 90×80 ($r \times \phi$) grid with three zones (20 ϕ intervals from 0 to 45 deg, 40 ϕ intervals from 45 to 135 deg, and 20 ϕ intervals from 135 to 180 deg) was used for the $\times$ fins. For the + fins, two zones were used (40 ϕ intervals from 0 to 90 deg and 40 ϕ intervals from 90 to 180 deg). To further improve the numerical accuracy, the Courant–Friedrichs–Lewy number, which controls the computational marching step, was set at 0.6.

The accuracy of the ZEUS code is well documented.[15,16] The accuracy of the numerical calculations was verified by comparing current results to the example case from Ref. 15. Additional tests were used to evaluate the numerical accuracy of the results. Results for $K_{W(B)}$ and $K_{B(W)}$ were compared for grids of 24×48, 60×60, and 90×80 with the difference in $K_{W(B)}$ of the order of 1.0% and the difference in $K_{B(W)}$ of the order of 1.5%. All of the results in this paper were obtained using a 90×80 grid. A looser grid could have been used for the Mach 8 and 10 cases because the bow shock was quite close to the body.

The current ZEUS solutions were calculated between the body and the bow shock. ZEUS has an option to specify boundary conditions at edge 3, outside the bow shock, and to capture the bow shock; however, this option was not used for the current calculations. At Mach 8 and 10 and large $S/R_{\rm LE}$, the fin tips extend through the bow shock. The lift from the fin area outside the bow shock was calculated using LPT as

$$\Delta L_{F,i} = \frac{4\alpha_\infty \cos\Theta_i q_\infty \Delta A_{F,i} \cos\Theta_i}{\sqrt{(M_\infty^2 - 1)}} \tag{18}$$

where the angle of attack of fin i differs from α_∞ by $\cos\Theta_i$ and the second $\cos\Theta_i$ converts the fin normal force to the missile lift force direction. $\Delta A_{F,i}$ is the area of fin i outside the bow shock. The total lift of fin i is the sum of the lift calculated by ZEUS and $\Delta L_{F,i}$, when the fin penetrates the bow shock. One must be careful in using the current results for $K_{W(B)}$ greater than about 3.5 in a semi-empirical code where bow shock effects are not included, because $K_{W(B)}$ accounts for the fin penetrating the bow shock.

Results and Discussion

Data for $K_{W(B)}$ and $K_{B(W)}$ are obtained at Mach 4, 6, 8, and 10 for $\gamma = 1.4$ and $\alpha_\infty = 2$ deg. The aspect ratio is 2.381 for $\epsilon = 30$ deg and 1.529 for $\epsilon = 20$ deg. $K_{W(B)}$ and $K_{B(W)}$ are plotted vs $S/R_{\rm LE}$, and the data over the whole body are plotted vs Z/R. The fin and body trailing edges were always coincident.

Figures 3 and 4 show contours of ΔP on the fin where ΔP is the difference between the nondimensional pressure underneath the fin and the nondimensional pressure on top of the fin. Figure 3 is for fin 1 and Fig. 4 is for fin 4 at Mach 4. The fin planform is bounded by the root chord at angle θ_f and the leading edge at angle ϵ. The trailing-edge location, Z/R, depends on the $S/R_{\rm LE}$ value of interest. The ΔP distributions are similar for both fins. Fin 4 has a higher ΔP over a slightly larger area than fin 1 due mainly to blockage of the crossflow on fin 1 by fin 4 especially near the root chord. This larger ΔP causes fin 4 to create a slightly larger lift than fin 1 for all fin sizes. Local flow conditions on the fins at $\Theta = 45$ and

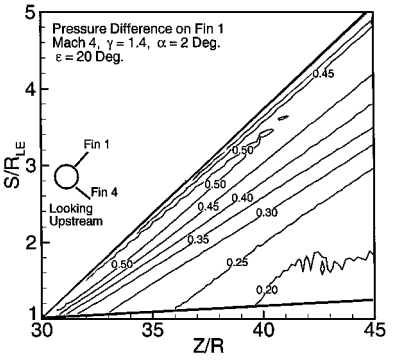

Fig. 3 Nondimensional pressure difference on fin 1 at Mach 4.

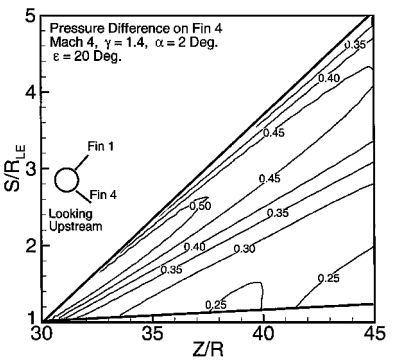

Fig. 4 Nondimensional pressure difference on fin 4 at Mach 4.

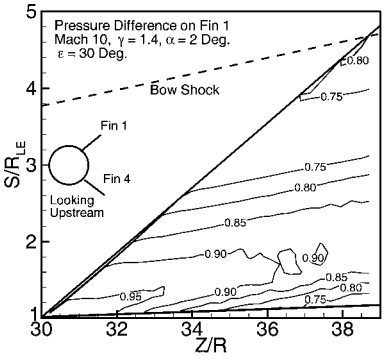

Fig. 5 Nondimensional pressure difference on fin 1 at Mach 10.

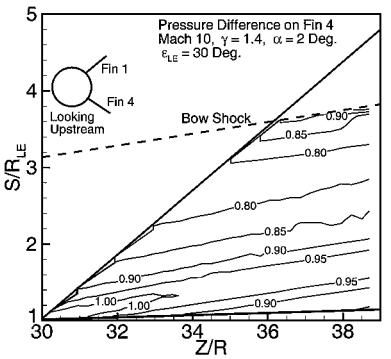

Fig. 6 Nondimensional pressure difference on fin 4 at Mach 10.

135 deg, that is, q greater than q_∞, may influence ΔP. In Ref. 17 it is stated that q_∞ can be assumed to be constant, independent of Θ, for crossflow Mach numbers less than about 0.5. The current cases have a maximum crossflow Mach number of $M_\infty \tan 2 \approx 0.35$, well below 0.50, so that changes in ΔP due to changes in dynamic pressure are negligible.

Figures 5 and 6 show ΔP contours on fin 1 and fin 4 at Mach 10. The bow shock position is also shown. The value of ΔP is roughly twice its value at Mach 4, and the highest ΔP values have moved inward, closer to the body. Fin 1 contacts the bow shock at $Z/R \approx 39$ ($S/R_{\rm LE} \approx 4.8$), whereas fin 4 contacts the bow shock at $Z/R \approx 36.3$ ($S/R_{\rm LE} \approx 3.6$). The angle of the center loop in the ΔP contours ($\Delta P \approx 0.50$ for $M_\infty = 4$ and $\Delta P \approx 1.0$ for $M_\infty = 10$) is approximately equal to the Prandtl–Meyer angle for a planer shock on a 1-deg ($\approx \Theta_f$) wedge.

Carryover, $K_{B(W)}$

The value of $K_{B(W)}$ is shown as a function of fin size, $S/R_{\rm LE}$, in Figs. 7 and 8 at Mach 4, 6, 8, and 10 for $\epsilon = 20$ and 30 deg, respectively. The SBT value of $K_{B(W)}$ is also shown.[14] The $K_{B(W)}$ data are considerably smaller than the SBT value. When $K_{B(W)}$ is zero the fins have no effect on the body lift. The value of $K_{B(W)}$ decreases as ϵ changes from 20 to 30 deg. $K_{B(W)}$ is always larger for $\times$ fins compared to $+$ fins. $K_{B(W)}$ increases as Mach number M_∞ increases. $K_{B(W)}$ is very sensitive to fin size, especially for small fins. Generally, $K_{B(W)}$ is positive, so that the effect of the fins is to increase the lift produced by the body. The trends in $K_{B(W)}$ agree with Ref. 7 (although the magnitude is smaller, because in Ref. 7 a slightly different definition for $K_{B(W)}$ is used). The $K_{B(W)}$ data are presented in the Appendix.

Carryover, $K_{W(B)}$

Values of $K^T_{W(B)}$ and $K^B_{W(B)}$ are shown as a function of $S/R_{\rm LE}$ in Figs. 9 and 10 at Mach 4, 6, 8, and 10 for $\epsilon = 20$ and 30 deg, respectively. Both $K^T_{W(B)}$ and $K^B_{W(B)}$ are less than 1, so that the wing-alone lift is greater than the lift produced by either the top set of fins or the bottom set of fins. As Mach number increases from 6 to 10, $K^T_{W(B)}$ and $K^B_{W(B)}$ decrease for a specific fin size, $S/R_{\rm LE}$. Recall that the lower fins hit the bow shock for $S/R_{\rm LE} \approx 3.6$ at Mach 10 for $\epsilon = 30$ deg. Also, near the bow shock the value of ΔP increases, so that the fin tips produce a rather large lift, tending to keep $K_{W(B)}$

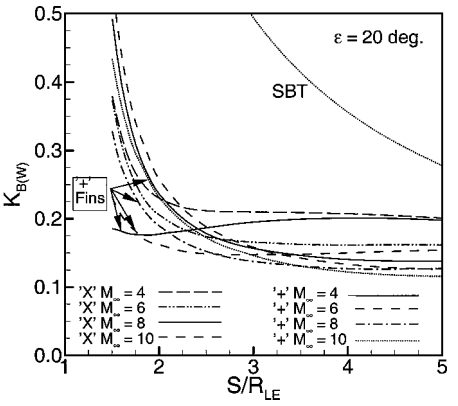

Fig. 7 $K_{B(W)}$ as a function of $S/R_{\rm LE}$ at $\epsilon = 20$ deg at Mach 4, 6, 8, and 10.

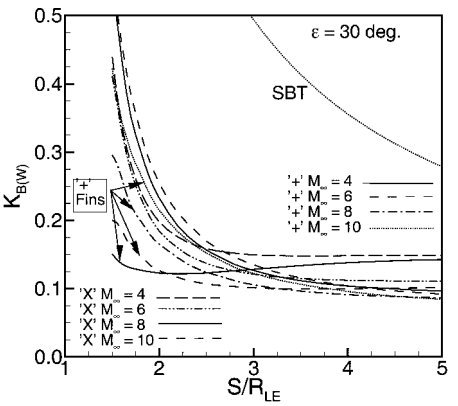

Fig. 8 $K_{B(W)}$ as a function of $S/R_{\rm LE}$ at $\epsilon = 30$ deg at Mach 4, 6, 8, and 10.

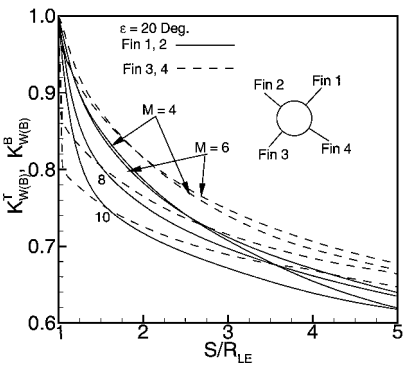

Fig. 9 $K^T_{W(B)}$ and $K^B_{W(B)}$ as a function of $S/R_{\rm LE}$ at Mach 4, 6, 8, and 10 for $\epsilon = 20$ deg.

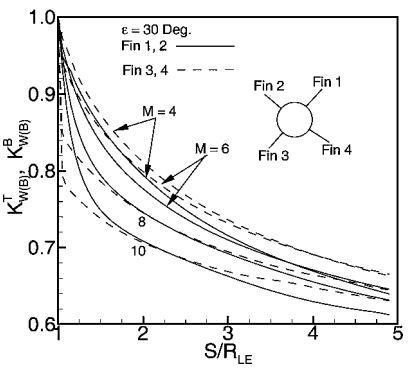

Fig. 10 $K^T_{W(B)}$ and $K^B_{W(B)}$ as a function of $S/R_{\rm LE}$ at Mach 4, 6, 8, and 10 for $\epsilon = 30$ deg.

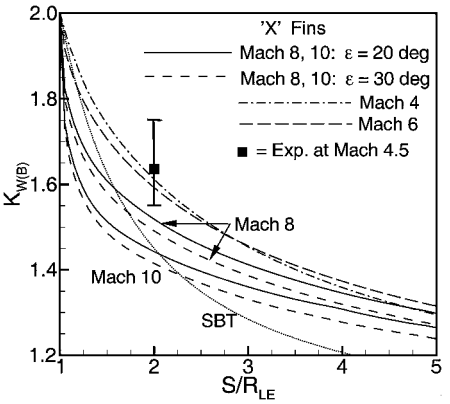

Fig. 11 $K_{W(B)}$ **for** $\times$ **fins as a function of** S/R_{LE} **at Mach 4, 6, 8, and 10 for** $\epsilon = 20$ **and 30 deg; experimental point is from data of Ref. 12.**

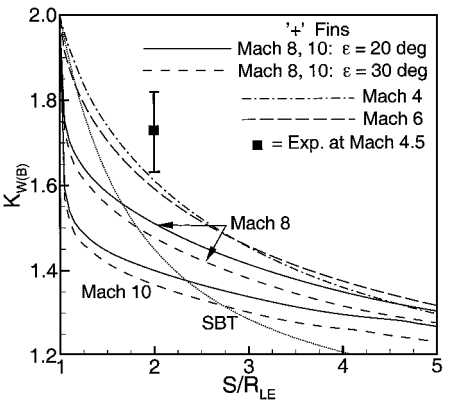

Fig. 12 $K_{W(B)}$ **for + fins as a function of** S/R_{LE} **at Mach 4, 6, 8, and 10 for** $\epsilon = 20$ **and 30 deg; experimental point is from data of Ref. 12.**

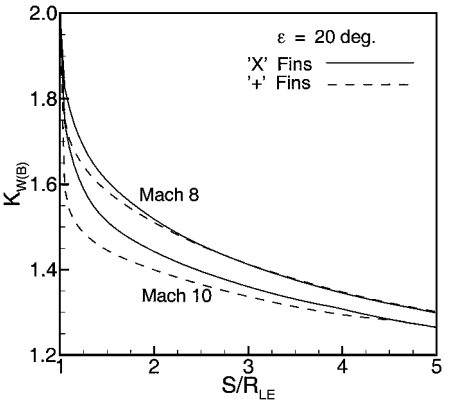

Fig. 13 $K_{W(B)}$ **as a function of** S/R_{LE} **at Mach 8 and 10 for** $\times$ **and + fins at** $\epsilon = 20$ **deg.**

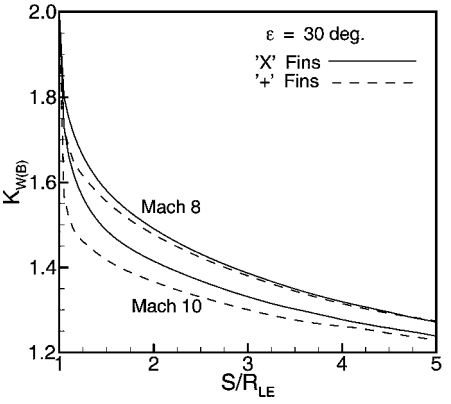

Fig. 14 $K_{W(B)}$ **as a function of** S/R_{LE} **at Mach 8 and 10 for** $\times$ **and + fins at** $\epsilon = 30$ **deg.**

large, which tends to cause $K^B_{W(B)}$ to level off at large S/R_{LE}. The Appendix presents equations for $K^T_{W(B)}$ and $K^B_{W(B)}$. The value of $K_{W(B)}$ [$K^T_{W(B)}$ plus $K^B_{W(B)}$] for $\times$ fins is shown as a function of S/R_{LE} and Mach number M_∞ in Fig. 11 for $\epsilon = 20$ and 30 deg. The four $\times$ fins produce more lift than the single wing alone over the entire range of S/R_{LE} because $K_{W(B)}$ is always greater than 1.

The value of $K_{W(B)}$ for + fins is shown as a function of S/R_{LE} and Mach number M_∞ in Fig. 12 for $\epsilon = 20$ and 30 deg. The values of $K_{W(B)}$ agree with the previous work of Ref. 7. At Mach 4 and 6 the $K_{W(B)}$ data did not change significantly with fin configuration nor ϵ. The data for $\times$ and + fins were the same to $\pm 2\%$; hence, $K_{W(B)}$ is assumed to be independent of roll at Mach 4 and 6 and all of the $K_{W(B)}$ data for $\times$ and + fins and $\epsilon = 20$ and 30 deg was averaged. The average value of $K_{W(B)}$ at Mach 4 and 6 is shown in Figs. 11 and 12. Figures 11 and 12 also show the SBT value for $K_{W(B)}$.[14] The SBT value drops off much faster with S/R_{LE} than the ZEUS calculations. The Appendix presents equations for $K_{W(B)}$.

Figures 11 and 12 contain an experimental data point from the Tri-Service database[12] for fin 51 at Mach 4.5 and $\alpha_\infty = 2.5$ deg. Fin 51 has $\epsilon = 26.6$ deg, $S/R_{LE} = 2$, and AR = 2 yielding $K_{W(B)} = 1.64$ ($\times$ fins) and $K_{B(W)} = 1.73$ (+ fins). The error bars represent the estimated experimental error. The experimental conditions are not the same as the current conditions, but the agreement with the numerical Mach 4 data is within 2% for $\times$ fins and within 7% for + fins.

Semivertex Angle

Figures 11 and 12 also show the effect of changing ϵ on $K_{W(B)}$. Recall that at Mach 4 and 6 $K_{W(B)}$ is independent of ϵ. Changing ϵ at Mach 8 and 10 produces about the same change in $K_{W(B)}$ for both $\times$ and + fin configurations. The $K_{W(B)}$ for $\epsilon = 30$ deg is slightly less than it is for $\epsilon = 20$ deg for all fin sizes. Consequently, as ϵ increases from 20 to 30 deg the lift for a given fin size decreases slightly.

Roll Orientation

Figures 13 and 14 show the effects of roll on the value of $K_{W(B)}$ for $\epsilon = 20$ and 30 deg, respectively. Only Mach 8 and 10 results are shown because roll does not effect $K_{W(B)}$ at Mach 4 and 6. At Mach 8, $K_{W(B)}$ is about the same for both fin configurations, whereas at Mach 10, $K_{W(B)}$ for $\times$ fins is slightly greater than it is for + fins. These trends are similar for both values of ϵ. At Mach numbers less than about 6, $\times$ and + fin configurations produce about the same lift. At Mach numbers greater than about 8, $\times$ fins produce more lift than + fins for the same finspan. In other words, rolling the missile 45 deg increases the lift slightly at speeds above Mach 8. This is different from the general trends stated in Ref. 2; however, here α_∞ is small, where the data from Ref. 2 (see Fig. 5 of Ref. 2) show that $\times$ fins produce slightly more lift than + fins. At high α_∞, the data given in Ref. 2 show that + fins produce more lift than $\times$ fins; consequently, the effects of roll angle on lift are influenced by α_∞.

Conclusions

The Euler predictions for $K_{W(B)}$ and $K_{B(W)}$ show the same general trends as the SBT predictions even though the SBT predictions do not depend on ϵ, Mach number, or $\times$ or + fin orientation. The carry-over factors vary with fin size in a manner similar to SBT predictions.

The analysis shows that $K^T_{W(B)}$ and $K^B_{W(B)}$ differ slightly, due to interference of the two lower fins on the flowfield around two upper fins. Normally, $K^B_{W(B)}$ is slightly greater than $K^T_{W(B)}$. Both $K^T_{W(B)}$ and $K^B_{W(B)}$ vary with Mach number, ϵ, and fin configuration. The values of $K^T_{W(B)}$ and $K^B_{W(B)}$ are less than 1 and increase to their theoretical value of 1 as S/R_{LE} decreases to 1. As M_∞ increases from 6 to 10 for a specific fin size, $K^T_{W(B)}$ and $K^B_{W(B)}$ decrease.

$K_{W(B)}$ is larger than the SBT value for all fin sizes and both fin configurations at Mach 4 and 6. At Mach 8 and 10, $K_{W(B)}$ is larger than the SBT value for S/R_{LE} greater than about 2 for both fin configurations. $K_{W(B)}$ is always greater than 1, so that the presence of the body produces a constructive influence on the wing lift.

$K_{B(W)}$ decreases with increasing fin size at a given Mach number. At given fin size, it is much smaller than the SBT value. The × fins yield a larger $K_{B(W)}$ than the + fins for the same fin size. $K_{B(W)}$ is always greater than zero, so that the presence of the fins positively effects the body lift.

For cruise conditions, the lift produced by the body–fin combination is a slight function of the roll angle. At lower Mach numbers, body–fin combinations with × and + fins produce about the same lift, whereas at higher Mach numbers body–fin combinations with × fins create more lift than body–fin combinations with + fins. For the body, × fins always produce slightly more body lift than the + fins. In general, a body–fin combinations will produce slightly more lift at a roll angle of 45 deg than it does at a roll angle of zero.

Appendix: Equations and Tables

The Appendix presents the equations that fit the $K_{W(B)}$ and $K_{B(W)}$ data shown in Figs. 9–12. The equations are 4th-degree polynomials of the form

$$F = A_0 + A_1 x + A_2 x^2 + A_3 x^3 + A_4 x^4 \tag{A1}$$

where $x = S/R_{\mathrm{LE}}$ and F is the carryover factor of interest. The equations are accurate to within 1% for $1.4 \le x \le 5$. Recall that the numerical data are not accurate at $S/R_{\mathrm{LE}} \le 1.4$. Table A1 gives the coefficients for the equations for $K^T_{W(B)}$ and $K^B_{W(B)}$ (Fig. 9) as a function of S/R_{LE} for $\epsilon = 20$ deg.

Table A2 gives the coefficients for the equations for $K^T_{W(B)}$ and $K^B_{W(B)}$ (Fig. 10) as a function of S/R_{LE} for $\epsilon = 30$ deg.

Table A3 gives the coefficients for the equations for $K_{W(B)}$ for the × fins as a function of S/R_{LE} for $\epsilon = 20$ and 30 deg (Fig. 11). At Mach 4 and 6 the equation is independent of ϵ and fin orientation.

Table A4 gives the coefficients for the equations for $K_{W(B)}$ for the + fins as a function of S/R_{LE} for $\epsilon = 20$ and 30 deg (Fig. 12). At Mach 4 and 6 the equation is independent of ϵ and fin orientation.

Table A5 gives values for $K_{B(W)}$ for the × and + fins as a function of S/R_{LE} for $\epsilon = 20$ deg (Fig. 7). The ZEUS data for S/R_{LE} less than 1.4 are not shown because they become inaccurate due to the small number of points on the fin.

Table A6 gives values for $K_{B(W)}$ for the × and + fins as a function of S/R_{LE} for $\epsilon = 30$ deg (Fig. 8). The ZEUS data for S/R_{LE} less

Table A1 Coefficients for $K^T_{W(B)}$ and $K^B_{W(B)}$ × fins, ϵ = 20 deg

		Coefficients				
Factor	M_∞	A_0	A_1	A_2	A_3	A_4
$K^T_{W(B)}$	4	1.282+0[a]	−4.677−1	1.569−1	−2.710−2	1.828−3
$K^T_{W(B)}$	6	1.322+0	−5.284−1	1.832−1	−3.093−2	1.996−3
$K^T_{W(B)}$	8	1.254+0	−5.238−1	1.990−1	−3.618−2	2.480−3
$K^T_{W(B)}$	10	1.191+0	−5.259−1	2.154−1	−4.157−2	2.994−3
$K^B_{W(B)}$	4	1.224+0	−3.504−1	9.805−2	−1.421−2	8.363−4
$K^B_{W(B)}$	6	1.207+0	−3.484−1	1.054−1	−1.648−2	1.019−3
$K^B_{W(B)}$	8	1.038+0	−2.381−1	6.964−2	−1.068−2	6.583−4
$K^B_{W(B)}$	10	9.440−1	−1.951−1	5.759−2	−8.236−3	4.282−4

[a] E+00 is indicated by +0.

Table A2 Coefficients for $K^T_{W(B)}$ and $K^B_{W(B)}$ × fins, ϵ = 30 deg

		Coefficients				
Factor	M_∞	A_0	A_1	A_2	A_3	A_4
$K^T_{W(B)}$	4	1.264+0[a]	−4.223−1	1.287−1	−1.992−2	1.211−3
$K^T_{W(B)}$	6	1.326+0	−5.558−1	2.016−1	−3.537−2	2.364−3
$K^T_{W(B)}$	8	1.254+0	−5.480−1	2.168−1	−4.085−2	2.884−3
$K^T_{W(B)}$	10	1.163+0	−5.010−1	2.043−1	−3.959−2	2.875−3
$K^B_{W(B)}$	4	1.289+0	−4.445−1	1.439−1	−2.357−2	1.511−3
$K^B_{W(B)}$	6	1.224+0	−3.941−1	1.270−1	−2.076−2	1.327−3
$K^B_{W(B)}$	8	1.035+0	−2.538−1	7.338−2	−1.074−2	6.138−4
$K^B_{W(B)}$	10	9.609−1	−2.405−1	7.834−2	−1.242−2	7.416−4

[a] E+00 is indicated by +0.

Table A3 Coefficients for $K_{W(B)}$ × fins, ϵ = 20 and 30 deg

		Coefficients				
ϵ	M_∞	A_0	A_1	A_2	A_3	A_4
20, 30	4	2.594+0[a]	−9.058−1	2.894−1	−4.705−2	3.006−3
20, 30	6	2.496+0	−8.557−1	2.845−1	−4.749−2	3.076−3
20	8	2.292+0	−7.619−1	2.686−1	−4.686−2	3.139−3
20	10	2.135+0	−7.209−1	2.730−1	−4.981−2	3.422−3
30	8	2.290+0	−8.018−1	2.902−1	−5.158−2	3.498−3
30	10	2.124+0	−7.415−1	2.826−1	−5.200−2	3.617−3

[a] E+00 is indicated by +0.

Table A4 Coefficients for $K_{W(B)}$ + fins, ϵ = 20 and 30 deg

		Coefficients				
ϵ	M_∞	A_0	A_1	A_2	A_3	A_4
20, 30	4	2.594+0	−9.058−1[a]	2.894−1	−4.705−2	3.006−3
20, 30	6	2.496+0	−8.557−1	2.845−1	−4.749−2	3.076−3
20	8	2.068+0	−5.157−1	1.681−1	−2.878−2	1.934−3
20	10	1.747+0	−3.393−1	1.018−1	−1.556−2	9.266−4
30	8	2.104+0	−6.061−1	2.114−1	−3.785−2	2.637−3
30	10	1.747+0	−3.393−1	1.018−1	−1.556−2	9.266−4

[a] E+00 is indicated by +0.

Table A5 $K_{B(W)}$, ϵ = 20, + and × fins

	+ Fins M_∞				× Fins M_∞			
S/R_{LE}	4	6	8	10	4	6	8	10
1.00	2.000	2.000	2.000	2.000	2.000	2.000	2.000	2.000
1.40	0.211	0.282	0.405	0.541	0.500	0.493	0.648	0.710
1.50	0.185	0.232	0.328	0.433	0.379	0.373	0.492	0.541
1.60	0.181	0.206	0.276	0.361	0.319	0.308	0.396	0.436
1.70	0.176	0.187	0.247	0.309	0.277	0.266	0.330	0.364
1.80	0.176	0.174	0.219	0.283	0.255	0.236	0.287	0.321
1.90	0.176	0.165	0.203	0.254	0.239	0.216	0.259	0.287
2.00	0.178	0.162	0.190	0.230	0.230	0.206	0.235	0.257
2.20	0.181	0.153	0.169	0.201	0.217	0.188	0.205	0.222
2.40	0.185	0.149	0.156	0.181	0.213	0.177	0.185	0.198
2.60	0.189	0.148	0.148	0.165	0.211	0.171	0.171	0.181
2.80	0.192	0.147	0.141	0.154	0.210	0.168	0.163	0.167
3.00	0.195	0.148	0.138	0.146	0.210	0.166	0.156	0.158
3.50	0.200	0.148	0.131	0.131	0.209	0.162	0.147	0.142
4.00	0.201	0.150	0.127	0.122	0.207	0.162	0.140	0.133
4.50	0.200	0.152	0.126	0.117	0.205	0.162	0.138	0.128
5.00	0.198	0.154	0.127	0.116	0.201	0.162	0.138	0.126

Table A6 $K_{B(W)}$, ϵ = 30, + and × fins

	+ Fins M_∞				× Fins M_∞			
S/R_{LE}	4	6	8	10	4	6	8	10
1.00	2.000	2.000	2.000	2.000	2.000	2.000	2.000	2.000
1.40	0.174	0.251	0.357	0.501	0.615	0.564	0.757	0.764
1.50	0.151	0.200	0.296	0.421	0.440	0.411	0.551	0.573
1.60	0.137	0.188	0.262	0.340	0.337	0.327	0.439	0.457
1.70	0.131	0.159	0.220	0.292	0.281	0.271	0.350	0.378
1.80	0.128	0.149	0.200	0.270	0.243	0.235	0.305	0.329
1.90	0.126	0.133	0.178	0.239	0.217	0.204	0.262	0.286
2.00	0.123	0.125	0.165	0.215	0.197	0.183	0.232	0.253
2.20	0.122	0.117	0.145	0.182	0.175	0.160	0.189	0.208
2.40	0.122	0.110	0.130	0.161	0.162	0.143	0.166	0.183
2.60	0.124	0.105	0.121	0.145	0.155	0.132	0.150	0.160
2.80	0.127	0.103	0.111	0.130	0.152	0.126	0.135	0.146
3.00	0.128	0.101	0.106	0.122	0.149	0.122	0.127	0.135
3.50	0.134	0.099	0.096	0.106	0.148	0.115	0.111	0.116
4.00	0.138	0.100	0.091	0.096	0.148	0.112	0.104	0.104
4.50	0.140	0.100	0.088	0.089	0.148	0.111	0.099	0.096
5.00	0.142	0.101	0.086	0.084	0.148	0.110	0.096	0.092

than 1.4 are not shown because they become inaccurate due to the small number of points on the fin.

References

[1]Hemsch, M. J., "Component Build-Up Method for Engineering Analysis of Missiles at Low-to-High Angles of Attack," *Tactical Missile Aerodynamics: Prediction Methodology*, edited by M. R. Mendenhall, Vol. 142, Progress in Astronautics and Aeronautics, AIAA, Washington, DC, 1992, pp. 115–169.

[2]Moore, F. G., and McInville, R. M., "Nonlinear Aeroprediction Methodology for Roll Position of 45 Degrees," *Journal of Spacecraft and Rockets*, Vol. 34, No. 1, 1997, pp. 54–61.

[3]Moore, F. G., McInville, R. M., and Hymer, T. C., "Application of the 1998 Version of the Aeroprediction Code," *Journal of Spacecraft and Rockets*, Vol. 36, No. 5, 1999, pp. 621–632.

[4]Burns, K. A., Deters, K. J., Stoy, S. L., Vukelich, S. R., and Blake, W. B., "Missile Datcom, User's Manual- Revision 6/93," Wright Lab., WL-TR-93-3043, Wright–Patterson AFB, OH, June 1993.

[5]Dillenius, M. F. E., Lesieutre, D. J., Hegedus, M. C., Perkins, S. C., Love, J. F., and Lesieutre, T. O., "Engineering, Intermediate, and High-Level Aerodynamic Prediction Methods and Applications," *Journal of Spacecraft and Rockets*, Vol. 36, No. 5, 1999, pp. 609–620.

[6]Wardlaw, A. B., Baltakis, F. P., and Priolo, F. J., "Space Marching Euler Solvers," *Tactical Missile Aerodynamics: Prediction Methodology*, edited by M. R. Mendenhall, Vol. 142, Progress in Astronautics and Aeronautics, AIAA, Washington, DC, 1992, pp. 379–444.

[7]Nelson, H. F., and Hillstrom, D. G., "Aerodynamic Interference for Hypersonic Missiles at Low Angle of Attack," *Journal of Spacecraft and Rockets*, Vol. 35, No. 6, 1998, pp. 749–754; "Errata," *Journal of Spacecraft and Rockets*, Vol. 36, No. 6, 1999, pp. 924, 925.

[8]Thomas, J. L., and Hartwich, P. M., "Navier–Stokes Analysis of Flows over Slender Airframes," *Tactical Missile Aerodynamics: Prediction Methodology*, edited by M. R. Mendenhall, Vol. 142, Progress in Astronautics and Aeronautics, AIAA, Washington, DC, 1992, pp. 561–648.

[9]Lesieutre, D. J., Mendenhall, M. R., Nazario, S. M., and Hemsch, M. J., "Prediction of the Aerodynamic Characteristics of Cruciform Missiles Including Effects of Roll Angle and Control Deflection," Nielsen Engineering and Research, Inc., NEAR TR-360, Mountain View, CA, Aug. 1987, pp. 18, 19.

[10]Stallings, R. L., Jr., and Lamb, M., "Wing-Alone Aerodynamic Characteristics for High Angles of Attack at Supersonic Speeds," NASA TP-1889, July 1981.

[11]Burns, K. A., and Bruns, K. D., "Development of an Improved Carryover Interference Method for Missile Datcom," AIAA Paper 96-3395, July 1996.

[12]Allen, J. M., "Tri-Service Missile Data Base," NASA Langley Research Center, (formal NASA documentation in process) transmitted to Univ. of Missouri, Rolla, MO, 1992.

[13]Nielsen, J. N., "Supersonic Wing–Body Interference at High Angles of Attack with Emphasis on Low Aspect Ratios," AIAA Paper 86-0568, Jan. 1986.

[14]Nielsen, J. N., *Missile Aerodynamics*, 2nd ed., Nielsen Engineering and Research, Mountain View, CA, 1988, pp 112–143.

[15]Wardlaw, A. B., and Priolo, F. J., "Applying the ZEUS Code," U.S. Naval Surface Weapons Center, NSWC TR 86-508, Dahlgren, VA, Dec. 1986.

[16]Priolo, F. J., and Wardlaw, A. B., "Euler Space-Marching Computations with Crossflow Separation for Missile-Type Bodies," AIAA Paper 90-0616, Jan. 1990.

[17]Hemsch, M. J., and Nielsen, J. N., "Aerodynamic Characteristics of Missile Control Fins in Nonlinear Flowfields," AIAA Paper 83-2083, Aug. 1983.

M. S. Miller
Associate Editor